Carbon 127 (2018) 170–176

Contents lists available at ScienceDirect

Carbon

journal homepage: www.elsevier.com/locate/carbon

Luminescent hybrid materials based on nanodiamonds

Dongxue Zhang [a], Qi Zhao [a, *], Jinhao Zang [a], Ying-Jie Lu [a], Lin Dong [a], Chong-Xin Shan [a, b, **]

[a] School of Physical Engineering, Zhengzhou University, Zhengzhou 450052, PR China
[b] State Key Laboratory of Luminescence and Applications, Changchun Institute of Optics, Fine Mechanics and Physics, Chinese Academy of Sciences, Changchun, 130033, PR China

ARTICLE INFO

Article history:
Received 5 February 2017
Received in revised form
29 April 2017
Accepted 3 November 2017
Available online 4 November 2017

ABSTRACT

Luminescent hybrid materials were prepared by covalently functionalizing nanodiamonds (NDs) with rare earth (RE) complexes. Pyromellitic acid (PMA), as the organic sensitizer, was grafted onto amino-terminated NDs to chelate lanthanide ions (Eu^{3+} and Tb^{3+}). The emission colors of the hybrid composite of ND-PMA-Eu_xTb_y can be tuned from red to orange, yellow and green by adjusting the molar ratio of Eu^{3+} to Tb^{3+}. Moreover, the luminescence of the hybrid composites exhibits remarkable photostability under ultraviolet irradiation for 60 h. As a proof-of-concept experiment, the as-synthesized ND-PMA-Eu and ND-PMA-Tb were employed as the phosphors for red and green light-emitting-diode (LED) devices with ultraviolet (UV) chips. Therefore, the nanodiamond-based luminescent hybrid material may find potential application in optical device.

1. Introduction

Nanodiamonds (NDs), as one of the most important carbon nanomaterials, have been traditionally used in lubrication, grinding, polishing and electroplating due to its high hardness and good thermal conductivity. Recently, with the development of preparation and purification technology, detonation NDs have attracted world-wide attention in optical and biomedical fields because of their rich surface groups, low toxicity, good biocompatibility, *etc* [1–3]. The most extensive study of luminescence centers in NDs is nitrogen-vacancy (N-V) defects [4]. However, the luminescence of N-V defects from detonation NDs is usually very poor due to the low nitrogen content and the surface graphite layer, which has become a huge obstacle that hinders their applications in bioimaging and light-emitting devices. Therefore, many efforts have been devoted to improve the fluorescence performance of NDs. Chang et al. proposed a method to increase the N-V concentration through irradiation by high-energy electron beam followed by an annealing in a vacuum at 800 °C [5]. However, this method usually requires high cost and complicated operations. What's more, it is difficult to produce high density color centers for detonation NDs due to the low nitrogen content [6,7]. Besides, NDs have been endowed with fluorescence by noncovalent or covalent modifications with dyes [8,9]. In addition, hydrophobic blue fluorescent NDs was also obtained through octadecylamine covalently attached onto carboxyl-modified NDs [10]. Nonetheless, the fluorescent dyes are involved in problems such as photobleaching and photo-blinking, which will limit NDs' utilization in luminescent devices. Therefore, it remains a tremendous challenge to develop an effective and facile method to NDs with intense and stable luminescence.

It is accepted that rare-earth (RE) compounds exhibit unique spectroscopic characteristics, such as long-lived excited states, large Stokes shift and sharp line-like emission. Especially, the lanthanide-based organic-inorganic hybrid materials show enhanced stability and improved luminescence by dispersing rare-earth complex in various matrices such as sol-gel-derived materials, mesoporous materials, clay minerals, which have found significant application in laser materials, optoelectronic devices and biological imaging, *etc* [11–15]. Inspired by these works, we envision if the luminescence of NDs can be enhanced by fabricating NDs-RE hybrid materials utilizing rare-earth complex as chromophores. Thus, the disadvantage of NDs, that is poor luminescence, can be avoided, and many potential applications of NDs may be pushed forward greatly.

* Corresponding author.
** Corresponding author. School of Physical Engineering, Zhengzhou University, Zhengzhou 450052, PR China.
E-mail addresses: zhaoqiv@126.com (Q. Zhao), cxshan@zzu.edu.cn (C.-X. Shan).

https://doi.org/10.1016/j.carbon.2017.11.009
0008-6223/

In this work, ND-based photoluminescent hybrid composites have been synthesized by exohedral functionalization of NDs with rare-earth complex. Pyromellitic acid (PMA) was grafted onto amino-terminated NDs which served as organic ligands to chelate RE ions and transfer exciting light to the RE ions efficiently. The ND-PMA-RE hybrid composites can emit multi-colored and considerably stable luminescence under ultraviolet (UV) illumination.

2. Experimental section

2.1. Reagents

Nanodiamonds (NDs) were purchased from Sino Crystal Micron Diamond Co. Ltd. (Zhengzhou, China). The coupling agent 3-Aminopropyltriethoxysilane (APTES), reducing agent sodium borohydride ($NaBH_4$), and pyromellitic dianhydride (PMDA) were purchased from Aladdin Chemistry Co. Ltd. (Shanghai, China). Europium oxide (Eu_2O_3) and Tetraterbiumheptaoxide (Tb_4O_7) were purchased from Beijing HWRK Chem Co.Ltd. (Beijing, China). N, N - Dimethylacetamide (DMAC) and N, N — Dimethylformamide (DMF) were purchased from Sinopharm Chemical Reagent Co.Ltd. (Shanghai, China). Ethyl alcohol absolute (C_2H_5OH) was purchased from Tianjin Yong Da Chemical Reagent Co.Ltd. (Tianjin, China). Concentrated nitric acid (HNO_3), sulfuric acid (H_2SO_4) and hydrochloric acid (HCl) were purchased from Luoyang Chemical Reagent. (Luoyang, China). Sodium hydroxide (NaOH), sodium carbonate (Na_2CO_3) and sodium bicarbonate ($NaHCO_3$) were purchased from Tianjin Sheng Ao Chemical Reagent Co.Ltd. (Tianjin, China).

2.2. Preparation of hybrid composites

2.2.1. Modification of NDs

The NDs were firstly carboxylated and oxidized according to previously reported techniques [16–18]. The NDs (0.2 g) were incubated at 425 °C for 30 min in muffle furnace, and put into mixed acid solution (60 mL, H_2SO_4: HNO_3 = 3: 1). The mixture was refluxed and stirred for 24 h at 80 °C. Then the product was cleaned with 0.1 M NaOH and HCl aqueous solution at 100 °C for 2 h, respectively, and labeled as ND-COOH. $NaBH_4$ (0.5 g) was added to the ND-COOH ethanol solution and refluxed at 60 °C for 24 h. The product was centrifugally washed with DMAC and labeled as ND-OH. The ND-OH was dispersed in anhydrous DMAC (40 mL) solution and placed in a two-necked flask under nitrogen. The APTES (1.2 mL) was added dropwise into the above mixture and stirred at room temperature for 48 h. Silanized NDs was obtained and labeled as ND-NH_2 after centrifugation and washing with DMF.

2.2.2. Connection of organic ligand

The ND-NH_2 was dispersed in DMF (40 mL) solution and placed in a two-necked flask under nitrogen atmosphere. Next, the PMDA (0.5 g) was added to the above mixture and stirred at 60 °C for 16 h. The product was marked as NDs-PMDA. Subsequently, to facilitate coordination with the RE ions, NDs-PMDA was put in a pH = 9.4 bicarbonate buffer solution for 2 h used for hydrolysis of PMDA. The product was labeled as ND-PMA after centrifugation, cleaning and drying process.

2.2.3. Preparation of ND-PMA-RE (RE^{3+} = Eu^{3+} and Tb^{3+})

$Eu(NO_3)_3$ and $Tb(NO_3)_3$ aqueous solutions were obtained by dissolving Eu_2O_3 and Tb_4O_7 into nitric acid, respectively. The ND-PMA (0.1 g) was added to the 0.01 M $RE(NO_3)_3$ (RE^{3+} = Eu^{3+} and Tb^{3+}) aqueous solution (20 mL) and stirred for 5 h. Ultimately, NDs-based rare earth hybrid luminescent materials were obtained after centrifugation and drying.

2.3. Characterization

Fourier transform infrared (FT-IR) spectroscopy was measured by KBr tablet using a Thermol Nicolet iz 10 spectrometer in the range of 4000–400 cm^{-1}. The Raman spectra of materials were recorded by Renishaw inVia Reflex Raman Microscope and Spectrometer. The composition of the materials was recorded by X-ray photoelectron energy spectra (XPS) using a Thermol Scientific Escalab 250Xi with Al Kα radiation. X-ray diffraction (XRD) patterns of the samples were recorded in a Rigaku D/MAX-3B diffractometer, and the morphologies of the samples were measured in a JEOL JSM-6700F field-emission scanning electron microscopy (FESEM). The solid - state luminescence spectrum and photostability of the luminescence were measured with a Hitachi F-7000 spectrometer, with a 150 W xenon lamp as the excitation source. The emission spectra of the LEDs were measured by Optical & Color & Electrical Parameters Integrated Test System using Starspec SSP6612. The luminescence decay curves were obtained from a Lecroy Wave Runner 6100 Digital Oscilloscope (1 GHz) using a tunable laser (pulse width = 4 ns, gate = 50 ns) as the excitation source (Continuum Sunlite OPO).

3. Results and discussion

3.1. Structure of ND-PMA-RE (RE^{3+} = Eu^{3+} and Tb^{3+})

Fig. 1 illustrates the process of surface modification of NDs and functionalization with RE. Firstly, The NDs surface was successively modified with homogenized carboxyl and hydroxyl groups by employing suitable oxidizing and reducing agents. Then, the PMDA was covalently bonded to the surface of the NDs by a dehydration condensation reaction between the amino and the carboxylic anhydride groups. The ND-PMA could coordinate with RE ions (Eu^{3+} and Tb^{3+}) after hydrolysis to produce the hybrid composite ND-PMA-RE.

The surface modification of NDs was monitored by FTIR spectroscopy. As shown in Fig. 2b, the absorption band at 1770, 1390 and 1256 cm^{-1} can be attributed to C=O stretching, O–H bending and C–O stretching mode of the carboxyl, respectively, indicating that the NDs have been carboxylated successfully [19,20]. The peaks located at 1568, 1048 and 800 cm^{-1} in Fig. 2c can be assigned to N–H scissor, C–N stretching and N–H bending mode, which suggests that the NDs have been terminated with amino groups. Further evidence for aminated NDs is the presence of stretching vibration mode of methylene at 2973 cm^{-1} and Si–O–Si stretching vibration at 1128 cm^{-1}. The peak at 1568 cm^{-1} shifts to 1580 cm^{-1} in Fig. 2d, which can be ascribed to the N–H bending mode of amide on ND-PMDA [21]. Meanwhile, the bands at 1716 cm^{-1} and 1772 cm^{-1} originate from the stretching vibration mode of C=O in carboxyl anhydride, which confirms that PMDA has been connected to the surface of the NDs. Furthermore, the peak corresponding to C=O shifts to 1760 cm^{-1} in Fig. 2e, suggesting that PMDA has been hydrolyzed to PMA. Hence, the carboxyl of PMA on the surface of the NDs can chelate RE^{3+} (Eu^{3+} and Tb^{3+}) to produce hybrid composite ND-PMA-RE.

XPS measurement was carried out to analyze the surface chemical composition of the ND-PMA-RE. Fig. 3a and c reveal that the ND-PMA-RE samples are mainly consisted of C, N, O, and RE (Eu or Tb). The peaks at 286.4, 400.1, 532.0 eV are ascribed to C 1s, N 1s, O 1s, respectively [20]. In addition, Eu 4d and Tb 4d are observed in the survey scan spectra [22–24]. The Eu 3d spectrum is shown in Fig. 3b, the spin-orbit splitting peaks of Eu 3d (Eu $3d_{5/2}$ and Eu $3d_{3/2}$) are observed at 1134.9 and 1164.6 eV, accompanied by two shake-down satellite peaks at 1154.9 and 1124.6 eV (labeled as 's') [25]. The peak at 1143.3 eV is the satellite peak from $3d4f^6$ multiplet

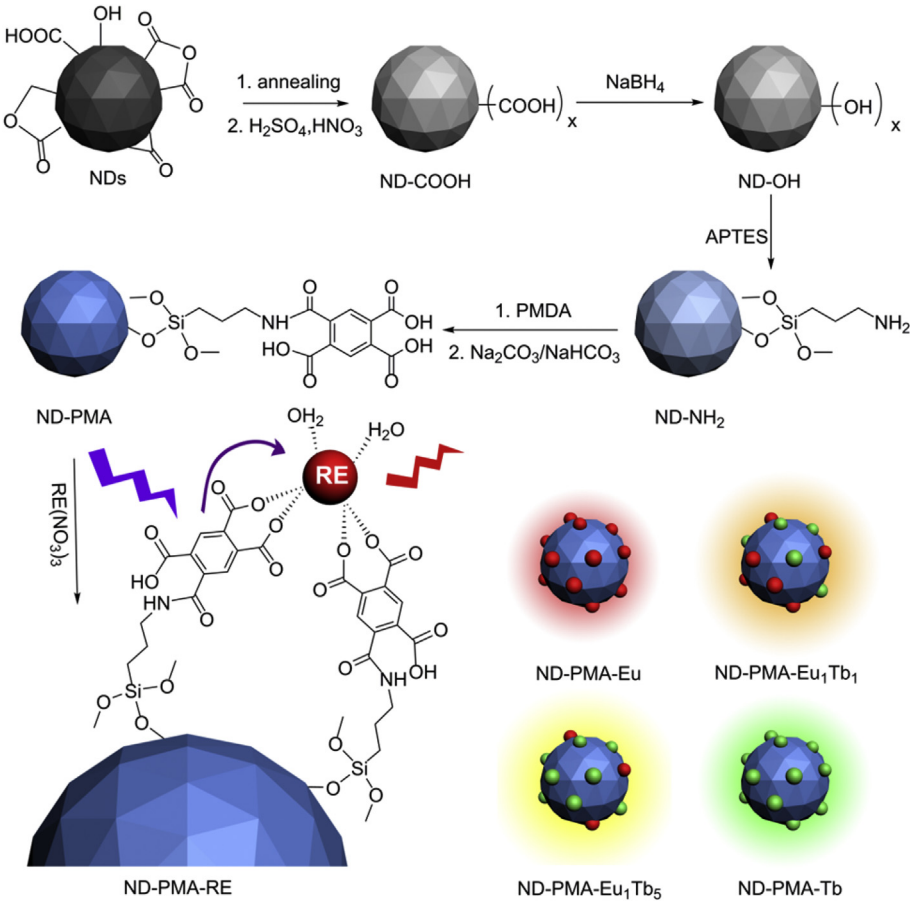

Fig. 1. Schematic illustration of the synthesis process of the ND-PMA-RE hybrid material. (A colour version of this figure can be viewed online.)

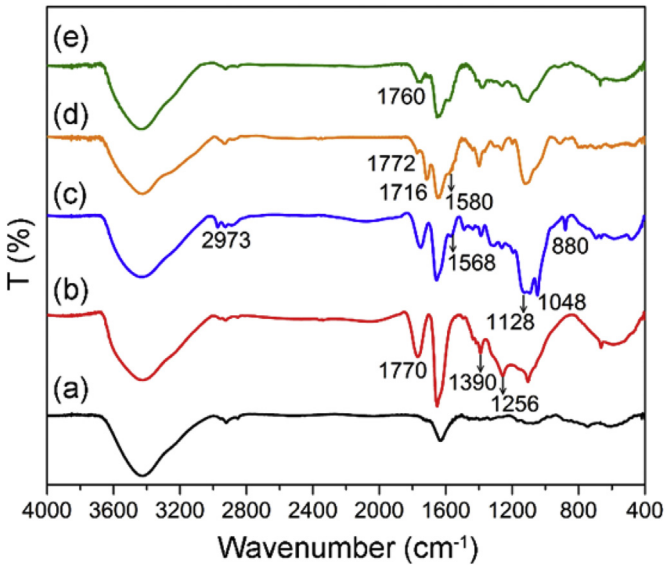

Fig. 2. FTIR spectra of the NDs raw materials (a), ND-COOH (b), ND-NH_2 (c), ND-PMDA (d) and ND-PMA (e). (A colour version of this figure can be viewed online.)

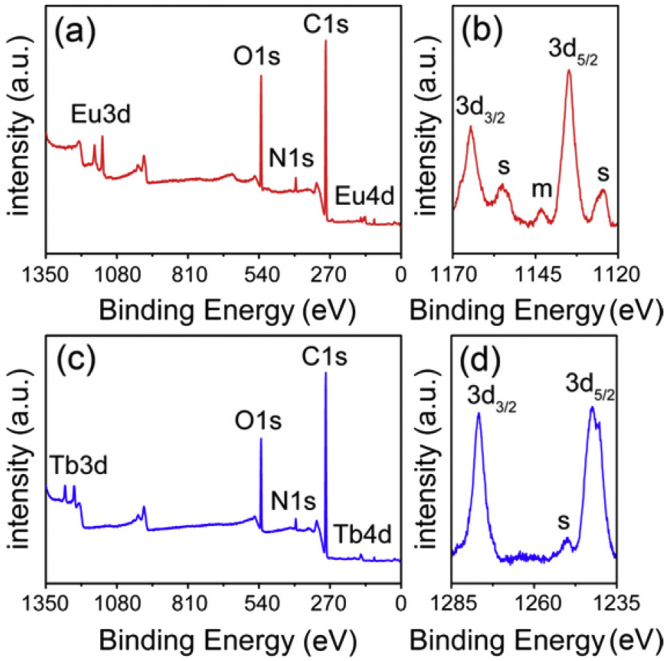

Fig. 3. XPS survey scan and RE 3d core level spectra of ND-PMA-Eu (a, b) and ND-PMA-Tb (c, d). (A colour version of this figure can be viewed online.)

structure of Eu^{3+} (labeled as 'm') [26]. The XPS spectrum of Tb 3d which is shown in Fig. 3d also exhibits two spin-orbits splitting peaks at 1242.0 and 1276.8 eV corresponding to Tb^{3+} $3d_{5/2}$ and Tb^{3+} $3d_{3/2}$ signals, respectively. A weak peak at 1250.2 eV is attributed to the satellite for the $3d_{5/2}$ component. The photoelectron lines of Eu 3d, Eu 4d, Tb 3d and Tb 4d indicate that the rare earth ions are in

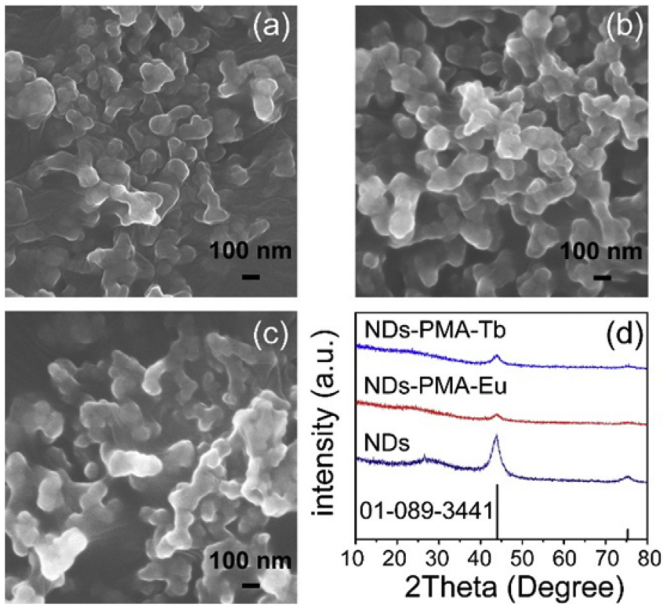

Fig. 4. FESEM images of the NDs (a), ND-PMA-Eu (b) and ND-PMA-Tb(c), as well as their XRD patterns (d). (A colour version of this figure can be viewed online.)

trivalent state [22]. The peak of C 1s at 286.4 eV can be attributed to the C—O or C—N from the ligands on the NDs surface [24]. Summarily, the results of XPS and FT-IR measurement verify that the rare earth ions have been covalently bonded with the NDs.

FESEM images of the NDs, ND-PMA-Eu and ND-PMA-Tb are depicted in Fig. 4a—c. The NDs and ND-PMA-RE are both consisted of nanospheres with an average diameter of 100 nm. The similarity in morphology suggests that the rare earth complex is covalently attached onto the NDs, rather than crystallized as a new phase. The XRD (Fig. 4d) of the NDs shows its characteristic peaks at $2\theta = 43.9°$ and 75.3°. The diffraction peaks become weaker in the ND-PMA-RE samples probably due to the ligand bonding. No impurity peaks are observed from the pattern of the hybrid composites, further suggesting that the NDs have been covalently functionalized by rare earth complex.

3.2. Luminescence performance of the ND-PMA-RE ($RE^{3+} = Eu^{3+}$ and Tb^{3+})

The excitation spectra for the ND-PMA-RE were obtained by monitoring the characteristic emissions of the Eu^{3+} and Tb^{3+} at 615 and 544 nm, respectively. As presented in Fig. S1, the broad band located at 260 and 290 nm is assigned to the effective overlap of $O^{2-} \rightarrow RE^{3+}$ charge transfer band (CTB) and π-π* electronic transitions of PMA organic ligand [27–29]. Under excitation of 260 nm, intense and characteristic emissions of the RE^{3+} were detected in the visible region for the ND-PMA-RE, while no emission peaks were observed for the original NDs (Fig. S2). Fig. 5a shows that the emission spectrum of the ND-PMA-Eu is composed of a group of lines peaking at 481, 492, 535, 555, 578, 591 and 615 nm, which can be ascribed to the $^5D_3 \rightarrow {}^7F_5$, $^5D_2 \rightarrow {}^7F_2$, $^5D_1 \rightarrow {}^7F_J$ (J = 1, 2) and $^5D_0 \rightarrow {}^7F_J$ (J = 0, 1, 2), respectively [30]. The hypersensitive transition $^5D_0 \rightarrow {}^7F_2$ at 615 nm is dominant and in charge of the bright red emission under UV-light irradiation with 254 nm (Fig. 5e). Moreover, the red/orange ratio ($^5D_0 \rightarrow {}^7F_2/{}^5D_0 \rightarrow {}^7F_1$) was 3.33, which suggests that the chemical environment around Eu^{3+} is non-rotationally symmetrical [31]. As shown in Fig. 5d, the emission peaks at 488, 544, 583 and 621 nm are explicitly assigned to $^5D_4 \rightarrow {}^7F_J$ (J = 6, 5, 4, 3) transitions of Tb^{3+}, in which the $^5D_4 \rightarrow {}^7F_5$ line is the prominent one and responsible for the bright green emission color under UV-light irradiation (Fig. 5h). The photoluminescence spectra of the ND-PMA-RE samples further confirm that the PMA molecules have been coordinated with RE ions and sensitized the activator ions greatly through 'antenna effect'. It is well known that the RE ions have low absorption cross section due to the forbidden 4f-4f transitions. Upon coordination with RE ions, the PMA ligand on the ND surface can absorb the excitation energy efficiently and transfer to the RE ions subsequently because of well-matched energy level between the triplet state of the ligand and the lowest excitation state of RE ion, which is the so-called antenna effect [32–34]. The excitation spectra of the Eu^{3+} and Tb^{3+} codoping hybrid composites (labeled as ND-PMA-Eu_xTb_y, Fig. S1c and d) are fundamentally identical to that of ND-PMA-Eu/Tb. The emission spectra show characteristic sharp bands of Tb^{3+} ($^5D_4 \rightarrow {}^7F_J$, J = 6, 5, 4) and Eu^{3+} ($^5D_0 \rightarrow {}^7F_J$, J = 0, 1, 2, 4) transitions (Fig. 5b and c). The emission colors of the ND-PMA-Eu_xTb_y could be simply tuned from orange to yellow by varying the molar ratio of Eu^{3+} to Tb^{3+}, as revealed in Fig. 5f and g. Furthermore, the chromaticity coordinates of the ND-PMA-RE hybrid materials were calculated, which fell well in the red, orange, yellow and green regions of 1931 CIE chromaticity diagram (Fig. 5i). In addition, the quantum yields of the ND-PMA-Tb and ND-PMA-Eu were measured to be 41.6% and 8.3%, respectively. As a proof-of-concept experiment, the ND-PMA-Eu and ND-PMA-Tb were coated on the UV chip (280 nm, 2 mW) to get UV-LEDs through encapsulation process. It is satisfactory that bright red and green light are achieved, respectively, as is demonstrated in Fig. 5j and k. The emission spectra of these two types of UV-LEDs and the contrast diagram of excitation spectra between ND-PMA-RE and UV chip are given in the Fig. 6.

Lifetime is an important parameter for luminescent materials in practical applications. As shown in Fig. 7, the decay curves of the ND-PMA-Eu, PMA-Eu, NDs-PMA-Tb and PMA-Tb can be fitted to a single exponential function as $I = I_0\exp(-t/\tau)$, where τ is the lifetime. The fluorescence lifetimes are determined to be 0.82, 0.92, 0.41, and 0.43 ms for the ND-PMA-Eu, ND-PMA-Tb, PMA-Eu and PMA-Eu, respectively. One can observe that the lifetimes of the ND-based hybrid material have been obviously prolonged compared with the pristine rare earth complexes. It can be speculated that the NDs matrix may restrict rotation and vibration of complexes which are covalently bonded to the surface of NDs and thereby reduce non-radiation deactivation process of the electron excitation state significantly [35,36]. The measured lifetime is related to the total relaxation rate by: $1/\tau = 1/\tau_0 + A_{nr}$ [37], where the τ_0 is the radiative lifetime and the A_{nr} is the nonradiative rate. Accordingly, the lifetime of the ND-PMA-RE can be increased when the nonradiative rate is reduced.

Photostability is one of the key factors in optical devices. The stability of the as-obtained hybrid materials (Fig. 8) were evaluated by direct exposure to 254 nm UV light (irradiation intensity 172.69 μW m^{-2}) for 60 h. The luminescence intensity of the ND-PMA-Tb (λ_{em} = 544 nm) was basically steady within 36 h and declined by 15.4% within 60 h. For the ND-PMA-Eu (λ_{em} = 615 nm), the luminescence intensity rapidly decreased by 26.3% within 12 h, followed by a relatively slow decrease within 60 h (46.0%). By contrast, the relative intensity of their complex counterparts, PMA-Eu and PMA-Tb, suffered a rapid decrease within 12 h (19.1% and 33.3%), which suggests that the ND matrix can enhance the photostability of rare earth complexes [38–43]. It is well-known that instability of rare earth complexes under UV irradiation is one of the problems in their application. The stability depends on the vibrations of the complex after absorbing light. The more intense the vibrations, the faster the decomposition of the complex. For the ND-PMA-Eu/Tb materials, strong covalent-bonding interactions of the rare-earth complex with NDs host material significantly limit

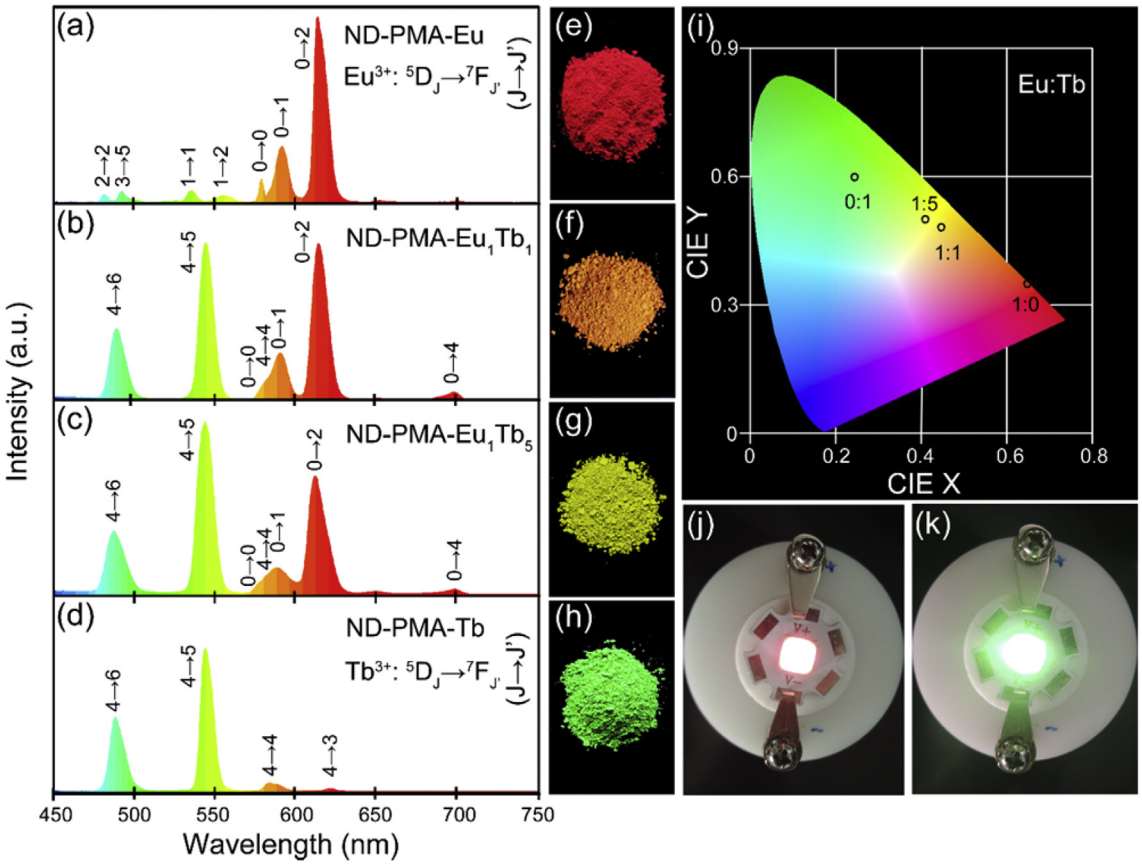

Fig. 5. Fluorescence spectra and corresponding images under 254 nm UV exposure of ND-PMA-Eu_xTb_y: (a, e) ND-PMA-Eu; (b, f) ND-PMA-Eu_1Tb_1; (c, g) ND-PMA-Eu_1Tb_5; (d, h) ND-PMA-Tb, respectively. (i) CIE chromaticity diagram of the hybrid materials. (j, k) Images of UV-LED coated with the ND-PMA-Eu and ND-PMA-Tb. (A colour version of this figure can be viewed online.)

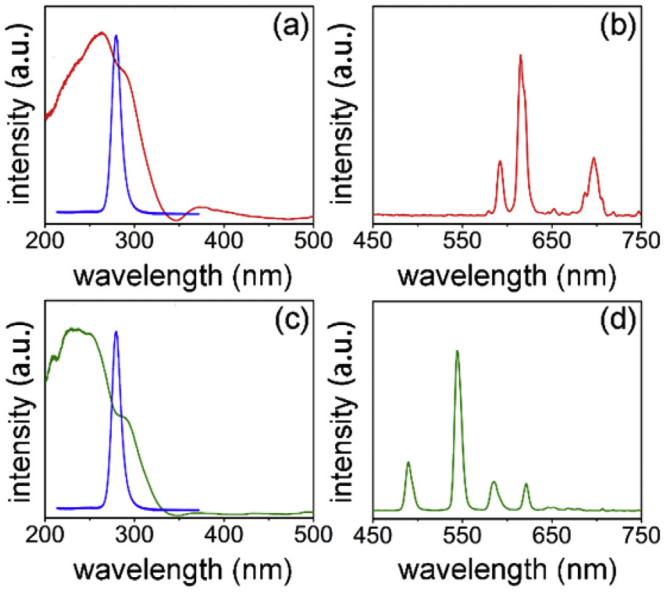

Fig. 6. (a) Comparison of the excitation spectra between ND-PMA-Eu (red) and UV chip (blue). (b) Emission spectrum of red LED lamp made from ND-PMA-Eu. (c) Comparison of the excitation spectra between ND-PMA-Tb (green) and UV chip (blue). (d) Emission spectrum of green LED lamp made from ND-PMA-Tb. (A colour version of this figure can be viewed online.)

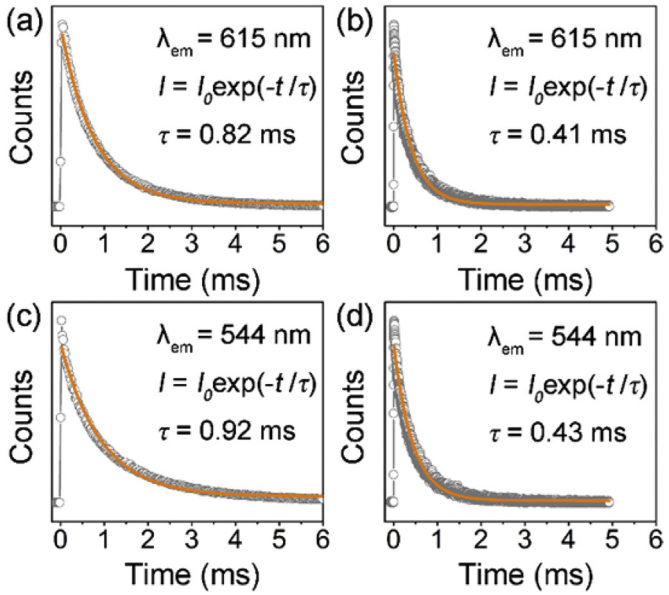

Fig. 7. The fluorescence decay curves of the ND-PMA-Eu (a), PMA-Eu (b), ND-PMA-Tb (c), PMA-Tb (d). (A colour version of this figure can be viewed online.)

the vibrations of the rare-earth complex and prevent the detrimental effect of various energy (C–H, C–C, or C–N) oscillators and intermolecular collisions between the complexes. As a consequence, the decomposition of the rare-earth complex is slowed significantly [39,44]. Furthermore, the as-synthesized hybrid

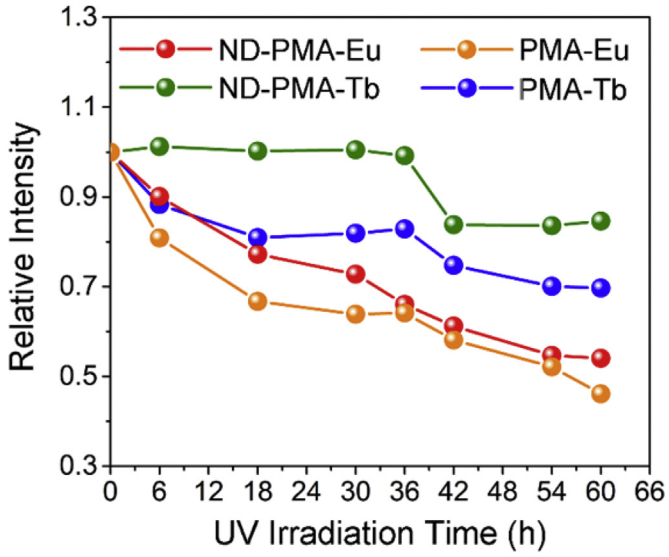

Fig. 8. Relative emission intensity of the ND-PMA-Eu, PMA-Eu, ND-PMA-Tb and PMA-Tb versus the irradiation time under 254 nm UV light. (A colour version of this figure can be viewed online.)

materials are quite competitive in photostability compared to previously reported rare earth-based fluorescent materials (Table S1). Overall, the ND-PMA-RE hybrid materials have good photostability under long term and high power UV light, which is a desirable property in designing luminescent devices.

4. Conclusions

In summary, luminescent hybrid materials (ND-PMA-RE) were synthesized by covalently modifying nanodiamonds (NDs) with pyromellitic acid (PMA) capable of coordinating to lanthanide ions. The emission colors of the ND-PMA-Eu_xTb_y could be simply tuned from red to green by varying the molar ratio of Eu^{3+} to Tb^{3+}. The hybrid composites ND-PMA-Eu and ND-PMA-Tb show longer lifetime of 0.82 and 0.92 ms than their complex counterparts PMA-RE. Remarkably, the ND-based hybrid materials possess good photostability under UV irradiation (254 nm, 172.69 μW m^{-2}). The color-tunable and photostable luminescence affords the hybrid material ND-PMA-RE a promising candidate for fabricating optical devices.

Acknowledgements

This work is financially supported by the Natural Science Foundation of China (11374296 and 21601159), the National Science Foundation for Distinguished Young Scholars of China (61425021), the China Postdoctoral Science Foundation (2016M590686).

Appendix A. Supplementary data

Supplementary data related to this article can be found at https://doi.org/10.1016/j.carbon.2017.11.009.

References

[1] V.N. Mochalin, O. Shenderova, D. Ho, Y. Gogotsi, The properties and applications of nanodiamonds, Nat. Nanotechnol. 7 (1) (2012) 11–23.
[2] Z. Cui, Y. Zhang, J. Zhang, H. Kong, X. Tang, L. Pan, et al., Sodium alginate-functionalized nanodiamonds as sustained chemotherapeutic drug-release vectors, Carbon 97 (2016) 78–86.
[3] J. Karpeta-Kaczmarek, M. Dziewięcka, M. Augustyniak, M. Rost-Roszkowska, Effects of short-term exposure of Acheta domesticus to nanodiamonds in food: DNA damage but no histological alteration in tissues, Carbon 110 (2016) 458–468.
[4] D. Tan, S. Zhou, B. Xu, P. Chen, Y. Shimotsuma, K. Miura, et al., Simple synthesis of ultra-small nanodiamonds with tunable size and photoluminescence, Carbon 62 (2013) 374–381.
[5] L.H. Chang, K. Chen, C.C. Chang, D.S. Tsai, C.C. Fu, T.S. Lim, et al., Mass production and dynamic imaging of fluorescent nanodiamonds, Nat. Nanotechnol. 3 (5) (2008) 284–288.
[6] O.A. Shenderova, I.I. Vlasov, S. Turner, G. Van Tendeloo, S.B. Orlinskii, A.A. Shiryaev, et al., Nitrogen control in nanodiamond produced by detonation shock-wave-assisted synthesis, J. Phys. Chem. C 115 (29) (2011) 14014–14024.
[7] C. Bradac, T. Gaebel, N. Naidoo, M.J. Sellars, J. Twamley, L.J. Brown, et al., Observation and control of blinking nitrogen-vacancy centres in discrete nanodiamonds, Nat. Nanotechnol. 5 (5) (2010) 345–349.
[8] S.C. Hens, G. Cunningham, T. Tyler, S. Moseenkov, V. Kuznetsov, O. Shenderova, Nanodiamond bioconjugate probes and their collection by electrophoresis, Diam. Relat. Mater. 17 (11) (2008) 1858–1866.
[9] A.M. Schrand, J.B. Lin, S.C. Hens, S.M. Hussain, Temporal and mechanistic tracking of cellular uptake dynamics with novel surface fluorophore-bound nanodiamonds, Nanoscale 3 (2) (2011) 435–445.
[10] V.M.Y. Gogotsi, Wet chemistry route to hydrophobic blue fluorescent nanodiamond, J. Am. Chem. Soc. 131 (13) (2009) 4594–4595.
[11] E.H. de Faria, E.J. Nassar, K.J. Ciuffi, M.A. Vicente, R. Trujillano, V. Rives, et al., New highly luminescent hybrid materials: terbium Pyridine–Picolinate covalently grafted on kaolinite, ACS Appl. Mater. Interfaces 3 (4) (2011) 1311–1318.
[12] S. Li-Ning, Z. Hong-Jie, M. Qing-Guo, L. Feng-Yi, F. Lian-She, P. Chun-Yun, et al., Near-infrared luminescent hybrid materials doped with lanthanide (Ln) complexes (Ln = Nd, Yb) and their possible laser application, J. Phys. Chem. B 109 (13) (2005) 6174–6182.
[13] J.P. Yu, D. Pal, R. Poole, R.A. Cann, M. J, A europium complex that selectively stains nucleoli of cells, J. Am. Chem. Soc. 128 (7) (2006) 2294–2299.
[14] S. Comby, D. Imbert, C. Vandevyver, J.C. Bunzli, A novel strategy for the design of 8-hydroxyquinolinate-based lanthanide bioprobes that emit in the near infrared range, Chem. Eur. J. 13 (3) (2007) 936–944.
[15] G. Chen, H. Qiu, P.N. Prasad, X. Chen, Upconversion nanoparticles: design, nanochemistry, and applications in theranostics, Chem. Rev. 114 (10) (2014) 5161–5214.
[16] M.H. Hsu, H. Chuang, F.Y. Cheng, Y.P. Huang, C.C. Han, J.Y. Chen, et al., Directly thiolated modification onto the surface of detonation nanodiamonds, ACS Appl. Mater. Interfac. 6 (10) (2014) 7198–7203.
[17] S. Osswald, G. Yushin, V. Mochalin, S.O. Kucheyev, Y. Gogotsi, Control of sp^2/sp^3 carbon ratio and surface chemistry of nanodiamond powders by selective oxidation in air, J. Am. Chem. Soc. 128 (35) (2006) 11635–11642.
[18] J.P. Goncalves, A.Q. Shaikh, M. Reitzig, D.A. Kovalenko, J. Michael, R. Beutner, et al., Detonation nanodiamonds biofunctionalization and immobilization to titanium alloy surfaces as first steps towards medical application, Beilstein J. Org. Chem. 10 (1) (2014) 2765–2773.
[19] G. Socrates, Infrared and Raman Characteristic Group Frequencies, third ed., John Wiley & Sons, New York, 2001.
[20] A.I. Ahmed, S. Mandal, L. Gines, O.A. Williams, C.L. Cheng, Low temperature catalytic reactivity of nanodiamond in molecular hydrogen, Carbon 110 (2016) 438–442.
[21] W. j. Zhang, X. f. Zou, J. f. Zhao, Preparation and performance of a novel graphene oxide sheets modified rare-earth luminescence material, J. Mater. Chem. C 3 (6) (2015) 1294–1300.
[22] S. Ghosh, K. Das, G. Sinha, J. Lahtinen, S.K. De, Bright white light emitting Eu and Tb co-doped monodisperse In_2O_3 nanocrystals, J. Mater. Chem. C 1 (35) (2013) 5557–5566.
[23] Z. Li, P. Wang, T. Yang, H. Yu, B. Xiao, M. Zhang, Enhanced luminescence with fast nanosecond lifetime in In_2S_3:Tb^{3+}Nanophosphors, J. Phys. Chem. C 119 (49) (2015) 27688–27694.
[24] J. Ryu, E. Lee, K. Lee, J. Jang, A graphene quantum dots based fluorescent sensor for anthrax biomarker detection and its size dependence, J. Mater. Chem. B 3 (24) (2015) 4865–4870.
[25] G.B. Lidia Armelao, Michele Pascolini, Michele Sessolo, Eugenio Tondello, Marco Bettinelli, Adolfo Speghini, Structure-luminescence correlations in europium-doped sol-gel ZnO nanopowders, J. Phys. Chem. C 112 (11) (2008) 4049–4054.
[26] E.C.S. Oh, Surface valence transition in trivalent Eu insulating compounds observed by photoelectron spectroscopy, Phys. Rev. B 59 (24) (1999) R15613–R15616.
[27] R. Pązik, A. Watras, L. Macalik, P.J. Dereń, One step urea assisted synthesis of polycrystalline Eu^{3+} doped KYP_2O_7 luminescence and emission thermal quenching properties, New J. Chem. 38 (3) (2014) 1129–1137.
[28] J. Wang, Y. Cheng, Y. Huang, P. Cai, S.I. Kim, H.J. Seo, Structural and luminescent properties of red-emitting Eu^{3+}-doped ternary rare earth antimonates R_3SbO_7 (R = La, Gd, Y), J. Mater. Chem. C 2 (28) (2014) 5559–5569.
[29] S.W. Li, H.J. Ren, S.G. Ju, Sensitized luminescence of LaF3:Eu3+ nanoparticles through pyromellitic acid, J. Nanosci. Nanotechnol. 14 (5) (2014) 3677–3682.
[30] T. Wang, P. Li, H. Li, Color-tunable luminescence of organoclay-based hybrid materials showing potential applications in white LED and thermosensors, ACS Appl. Mater. Interfac. 6 (15) (2014) 12915–12921.
[31] M. Fernandes, V. de Zea Bermudez, R.A. Sá Ferreira, L.D. Carlos, A. Charas, J. Morgado, et al., Highly photostable luminescent poly(ε-caprolactone)

siloxane biohybrids doped with europium complexes, Chem. Mater. 19 (16) (2007) 3892–3901.
[32] Heejin Jeong, B.-I. L, Song-Ho Byeon, Antenna effect on the organic spacer-modified Eu-doped layered gadolinium hydroxide for the detection of vanadate ions over a wide pH range, ACS Appl. Mater. Interfac. 8 (17) (2016) 10946–10953.
[33] S.I. Klink, L. Grave, D.N. Reinhoudt, F.C.J.M.V. Veggel, M.H.V. Werts, F.A.J. Geurts, et al., A systematic study of the photophysical processes in polydentate triphenylene-functionalized Eu^{3+}, Tb^{3+}, Nd^{3+}, Yb^{3+}, and Er^{3+} complexes, J. Phys. Chem. A 104 (23) (2000) 5457–5468.
[34] B. Gao, L. Fang, R. Zhang, J. Men, Preparation of aromatic carboxylic acid-functionalized polysulfone and preliminary exploration of fluorescence emission character of formed polymer-rare earth complexes, Synth. Met. 162 (5–6) (2012) 503–510.
[35] S. Gago, J.A. Fernandes, J.P. Rainho, R.A. Sá Ferreira, M. Pillinger, A.A. Valente, et al., Highly luminescent tris(β-diketonate)europium(III) complexes immobilized in a functionalized mesoporous silica, Chem. Mater. 17 (20) (2005) 5077–5084.
[36] Shi-Jie Wang, Jiang-Bo Hu, Yin-Yin Wang, Fang Luo, Coating graphene oxide sheets with luminescent rare-earth complexes, J. Mater. Sci. 48 (2) (2013) 805–811.
[37] Ji Yeon Han, Won Bin Im, Ga-yeon Lee, Duk Young Jeon, Near UV-pumped yellow-emitting Eu^{2+}-doped $Na_3K(Si_{1-x}Al_x)_8O_{16\pm\delta}$ phosphor for white-emitting LEDs, J. Mater. Chem. 22 (18) (2012) 8793–8798.
[38] J. Kai, M.C.F.C. Felinto, L.A.O. Nunes, O.L. Malta, H.F. Brito, Intermolecular energy transfer and photostability of luminescence-tuneable multicolour PMMA films doped with lanthanide–β-diketonate complexes, J. Mater. Chem. 21 (11) (2011) 3796–3802.
[39] W.A. Dar, K. Iftikhar, Phase controlled colour tuning of samarium and europium complexes and excellent photostability of their PVA encapsulated materials. Structural elucidation, photophysical parameters and the energy transfer mechanism in the Eu^{3+} complex by Sparkle/PM3 calculations, Dalton Trans. 45 (21) (2016) 8956–8971.
[40] A. Revaux, G. Dantelle, N. George, R. Seshadri, T. Gacoin, J.P. Boilot, A protected annealing strategy to enhanced light emission and photostability of YAG: Ce nanoparticle-based films, Nanoscale 3 (2011) 2015–2022.
[41] S. Takeshita, T. Watanabe, T. Isobe, T. Sawayama, S. Niikura, Improvement of the photostability for YVO_4 : Bi^{3+}, Eu^{3+} nanoparticles synthesized by the citrate route, Opt. Mater. 33 (2011) 323–326.
[42] P.P. Lima, R.A. Sá Ferreira, R.O. Freire, F.A. Almeida Paz, L. Fu, S. Alves, et al., Spectroscopic study of a UV-photostable organic-inorganic hybrids incorporating an Eu^{3+} β-diketonate complex, ChemPhysChem 7 (3) (2006) 735–746.
[43] M. Fernandes, V.D.Z. Bermudez, R.A.S. Ferreira, L.D. Carlos, A. Charas, J.M. Morgado, M. Silva, M.J. Smith, Highly photostable luminescent poly (ε-caprolactone) siloxane biohybrids doped with europium complexes, Chem. Mater. 19 (2007) 3892–3901.
[44] Qinghong Xu, Liansheng Li, Xinsheng Liu, Ruren Xu, Incorporation of rare-earth complex $Eu(TTA)_4C_5H_5NC1_6H_{33}$ into surface-modified S-MCM-41 and its photophysical properties, Chem. Mater. 14 (2) (2002) 549–555.